Optical Engineering

OpticalEngineering.SPIEDigitalLibrary.org

Single weakly tilted FBG in 2-μm band capable of measuring temperature, axial strain, and surrounding refractive index

Dan Cheng
Fengping Yan
Ting Feng
Zhuoya Bai
Luna Zhang
Wei Wang
Shuo Liu
Hong Zhou
Yafei Hou

SPIE.

Dan Cheng, Fengping Yan, Ting Feng, Zhuoya Bai, Luna Zhang, Wei Wang, Shuo Liu, Hong Zhou, Yafei Hou, "Single weakly tilted FBG in 2-μm band capable of measuring temperature, axial strain, and surrounding refractive index," *Opt. Eng.* **57**(9), 096107 (2018), doi: 10.1117/1.OE.57.9.096107.

Single weakly tilted FBG in 2-μm band capable of measuring temperature, axial strain, and surrounding refractive index

Dan Cheng,[a] Fengping Yan,[a,*] Ting Feng,[b] Zhuoya Bai,[a] Luna Zhang,[a] Wei Wang,[a] Shuo Liu,[c] Hong Zhou,[d] and Yafei Hou[e]
[a]Beijing Jiaotong University, Institute of Lightwave Technology, Key Laboratory of All Optical Network and Advanced Telecommunication of EMC, Beijing, China
[b]Hebei University, College of Physics Science and Technology, Photonics Information Innovation Center, Hebei Key Lab of Optic-Electronic Information and Materials, Baoding, China
[c]Hebei University of Technology, School of Electronic Information Engineering, Tianjin, China
[d]Osaka Institute of Technology, Department of Electronics, Information and Communication Engineering, Osaka, Japan
[e]Okayama University, Graduate School of Natural Science and Technology, Okayama, Japan

Abstract. Optical fiber devices and applications in the 2-μm band have been investigated extensively due to its unique advantages, such as eye safety. A fiber sensor based on tilted fiber Bragg grating with a grating plane angle of 2 deg is fabricated and experimentally tested. To the best of the authors' knowledge, this is the first tilted fiber Bragg grating sensor to realize simultaneous measurements of temperature, axial strain, and a certain range of surrounding refractive index (SRI) at the 2-μm band. This paper uses the wavelength detection method and selects three independent resonant wavelengths as the investigated parameters. Results show that perturbations of temperature, axial strain, and SRI can shift the wavelengths of the core mode resonance and cladding mode resonance to some degree. The temperature sensitivities of the core mode and cladding mode are nearly the same, but their axial-strain sensitivities are different. Furthermore, the core mode is insensitive to the change in SRI. The sensitivities of SRI, temperature, and strain can thus be obtained by experimentally determining the wavelength shifts of the three independent resonance peaks. A 3×3 matrix containing the relationship coefficients between the disturbances of temperature, axial strain, and SRI and wavelength shifts is constructed. By reversely solving the matrix equation, variations in temperature, strain, and SRI can be obtained using the experimental determination of wavelength drifts. [DOI: 10.1117/1.OE.57.9.096107]

Keywords: tilted fiber Bragg grating; 2-μm band; fiber-optic sensors.

Paper 180028 received Jan. 5, 2018; accepted for publication Aug. 22, 2018; published online Sep. 13, 2018.

1 Introduction

Relevant theoretical and experimental research on fiber applications in the 2-μm band of the optical spectrum is developing rapidly. Among them, Tm^{3+} and Ho^{3+} ion-doped glass fiber materials have demonstrated notable gains in bandwidth ranging from 1.7 to 2.1 μm. This bandwidth provides a broad selectable range of laser operating wavelengths in the eye-safe spectral region[1] and shows excellent overlap with the absorption lines of various atmospheric gases, such as H_2O, CO_2, and liquid water. Therefore, fiber devices in this band range are suitable for CO_2 detection[2] and other sensing measurements. Lasers operating in this band are also easily absorbed by biological tissue and can be used in superficial surgery.[3] When the 2-μm band laser is transmitted through optical fibers or based endoscopes, surgery becomes more precise and controllable if a sensor provided for temperature and the strain or surrounding refractive index (SRI) is available. Similarly, this type of sensing device can be used in many other medical disciplines. In addition, fiber devices operating in the 2-μm band are used in biology, laser radar, remote sensing detection, military technology, and other fields.[4–7] However, due to imperfect fabrication technology, optical fiber sensing research in the 2-μm band is still in an experimental stage[8] and requires deeper exploration. A few fiber Bragg grating (FBG) sensors operating in this band have been reported in the literature. FBG often serves as a functional device that is particularly important in fiber applications, such as fiber laser and fiber sensing. Therefore, FBG-based sensors working in the 2-μm band warrant urgent research.

Sensors measuring temperature, axial strain, and SRI are essential to the fields of biochemical engineering, environmental monitoring, and medical science. Optical fiber sensors have received widespread attention due to their impressive superiority in compact size, fast response, and high operability.[9] In optical fiber sensing, the employment and research interests in fiber gratings are quite common, which are mainly used in strain, temperature and humidity measurement.[10–14] However, the Bragg wavelength is both sensitive to the change of strain and temperature, which will make it hard to eliminate the crossing-sensitivity impact. To overcome this obstacle, a common approach is to use two or more gratings that characterize different strain and temperature sensitivity; however, this technique increases the complexity of the entire operating system.[15,16] For SRI measurement, an FBG must often be corroded to a certain extent and then become more fragile.[17] Although long-period fiber grating (LPFG) exhibits excellent performance in SRI measurement,[18] the high cross-sensitivity to surrounding

*Address all correspondence to: Fengping Yan, E-mail: fpyan@bjtu.edu.cn

environmental perturbation cannot be ignored.[19] These drawbacks can be successfully overcome using tilted fiber Bragg grating (TFBG) owing to its unique physical structure. In TFBG, grating planes are blazed at an angle with respect to the fiber-propagating axis; as such, light transmitted in the fiber couples with the core mode as well as backward-propagating cladding modes, leading to a series of dense, comb-like spectral resonances that can be excited and are located behind the Bragg wavelength.[20,21] Because the sensitivity to environmental disturbances between core–core mode resonance and core–cladding mode resonance is different,[22–24] multiparameter simultaneous measurement can be realized with a single TFBG. In general, TFBG combines the advantages of FBG and LPFG[25,26] and demonstrates great potential in simultaneous measurement of various parameters.

This paper proposes and experimentally tests a simple TFBG fiber sensor operating in the 2-μm band that can realize simultaneous measurement of temperature, axial strain, and a certain SRI range. The perturbations of temperature, axial strain, and SRI can lead to a shift in the core mode resonance and cladding mode resonance to some degree. The temperature sensitivities of the core mode and cladding mode are nearly identical, but their strain sensitivities are different. Furthermore, the core mode is insensitive to changes in SRI. By reversely solving the sensitivity coefficients matrix constructed using these three parameters, changes in SRI, temperature, and axial strain can be determined by observing the spectral shifts of different independent resonance peaks.

2 Theory of Tilted Fiber Bragg Grating Sensing Mechanism

Figure 1 shows the structure of the TFBG, which belongs to short-period fiber grating. Similar to FBG, TFBG also features a Bragg wavelength. Because the grating plane forms a tilt angle relative to the fiber-propagating axis, the core mode light can couple easily with the cladding modes. In other words, when light is guided into the TFBG, coupling occurs not only between the forward- and backward-propagating core modes but also between the forward-propagating core mode and the backward-propagating cladding modes.[27] As the cladding has a larger diameter than the fiber core, several cladding modes can be excited.[28] As shown in Fig. 2, behind the Bragg wavelength, a series of dense, comb-like cladding mode resonances can be clearly observed from the transmission spectrum. The resonance wavelengths can be deduced from the phase-matching condition and expressed as follows:

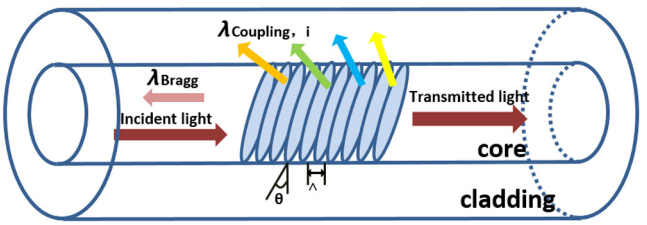

Fig. 1 Three-dimensional schematic plot of the configuration of grating integrated in fiber core.

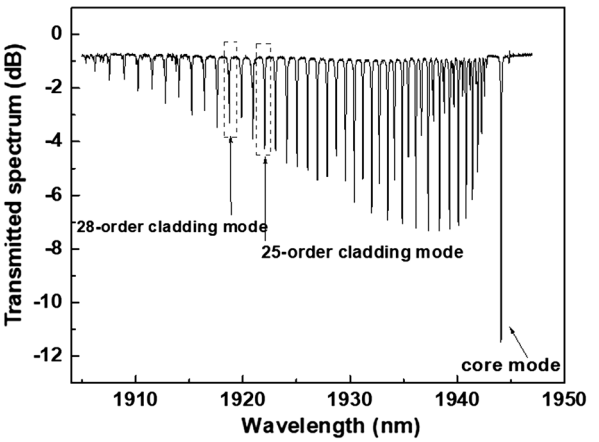

Fig. 2 Transmission spectra of homemade TFBG with a tilt angle of 2 deg.

$$\lambda_B = 2n_{\text{eff}}^{co}\Lambda_g, \tag{1}$$

$$\lambda_{cl}^{i} = (n_{\text{eff}}^{co} + n_{\text{eff}}^{cl,i})\Lambda_g, \tag{2}$$

where $\Lambda_g = \frac{\Lambda}{\cos\theta}$, θ is the tilt angle, Λ is the normal grating period, Λ_g is the grating period along the axis, and n_{eff}^{co} and $n_{\text{eff}}^{cl,i}$ denote the effective refractive indices of the core mode and i'th cladding mode, respectively.

The effective refractive index and grating period of the TFBG can be influenced by changes in temperature and axial strain. Specifically, the thermos-optic coefficient represents the quantitative relationship between the effective refractive index variation of the TFBG and the change of temperature, whereas the thermal expansion coefficient denotes the same relationship of the grating period variation of the TFBG induced by a change in temperature. In this case, the values of the two coefficients are low, which causes the resonance peak of each mode shift to a longer wavelength to nearly the same extent with an increase in the temperature.[29] In terms of strain effect, the resonant wavelength of each mode exhibits a different wavelength shift under the same strain due to different photoelastic constants. Furthermore, when the cladding modes propagate within the interface region between the cladding and the external environment, the effective refractive indices are also sensitive to the ambient refractive index. Higher cladding modes have a larger power ratio in the evanescent field to the surrounding environment and are thus more sensitive to changes in SRI.[27] With a continuous increase in the SRI, the highest order cladding modes are affected first. Their corresponding resonant wavelengths move toward a longer wavelength.[27] Wavelength drifts of certain cladding-guided modes increase monotonically with an increase in SRI until the resonant wavelength satisfies the cut-off condition; that is, the extent of resonant wavelength drift induced by the change in SRI is enhanced with an increase in SRI, and the SRI sensitivity reaches its maximum when the cladding mode satisfies the cut-off condition,[24] whereas the core mode is confined in the core, it is not affected by SRI. Variations in temperature, axial strain, and SRI can be determined according to the wavelength shifts of various independent resonance peaks before the cladding modes satisfy the cut-off condition.

Variations in the resonance wavelengths induced by the change of temperature ΔT, axial strain $\Delta\varepsilon$, and SRI Δn_{ext} can be given by Ref. 15:

$$\begin{aligned}\frac{\Delta\lambda_B}{\lambda_B} &= \left(\frac{1}{n_{\text{eff}}}\frac{\partial n_{\text{eff}}}{\partial T}+\frac{1}{\Lambda_B}\frac{\partial\Lambda_B}{\partial T}\right)\Delta T \\ &+\left(\frac{1}{\Lambda_B}\frac{\partial\Lambda_B}{\partial\varepsilon}+\frac{1}{n_{\text{eff}}}\frac{\partial n_{\text{eff}}}{\partial\varepsilon}\right)\Delta\varepsilon \\ &+\left(\frac{1}{\Lambda_B}\frac{\partial\Lambda_B}{\partial n_{\text{ext}}}+\frac{1}{n_{\text{eff}}}\frac{\partial n_{\text{eff}}}{\partial n_{\text{ext}}}\right)\Delta n_{\text{ext}} \\ &= K_{B,T}\Delta T+K_{B,\varepsilon}\Delta\varepsilon+K_{B,n_{\text{ext}}}\Delta n_{\text{ext}}, \end{aligned} \tag{3}$$

$$\begin{aligned}\frac{\Delta\lambda_{cl}^{i}}{\lambda_{cl}^{i}} &= \left[\frac{1}{n_{\text{eff}}^{co}+n_{\text{eff}}^{cl,i}}\frac{\partial(n_{eff}^{co}+n_{eff}^{cl,i})}{\partial T}+\frac{1}{\Lambda}\frac{\partial\Lambda}{\partial T}\right]\Delta T \\ &+\left[\frac{1}{\Lambda}\frac{\partial\Lambda}{\partial\varepsilon}+\frac{1}{n_{\text{eff}}^{co}+n_{\text{eff}}^{cl,i}}\frac{\partial(n_{eff}^{co}+n_{eff}^{cl,i})}{\partial\varepsilon}\right] \\ &+\left[\frac{1}{\Lambda}\frac{\partial\Lambda}{\partial n_{\text{ext}}}+\frac{1}{n_{\text{eff}}^{co}+n_{\text{eff}}^{cl,i}}\frac{\partial(n_{\text{eff}}^{co}+n_{\text{eff}}^{cl,i})}{\partial n_{\text{ext}}}\right]\Delta n_{\text{ext}} \\ &= K_{cl,T}^{i}\Delta T+K_{cl,\varepsilon}^{i}\Delta\varepsilon+K_{cl,n_{\text{ext}}}^{i}\Delta n_{\text{ext}}, \end{aligned} \tag{4}$$

where $K_{B,T}$ and $K_{cl,T}^{i}$, $K_{B,\varepsilon}$ and $K_{cl,\varepsilon}^{i}$, and $K_{B,n_{\text{ext}}}$ and $K_{cl,n_{\text{ext}}}^{i}$ are the temperature coefficients, axial-strain coefficients, and refractive coefficients, respectively, for the core mode and i'th cladding mode. As the core mode is insensitive to the change in SRI, $K_{B,n_{\text{ext}}}=0$. To achieve three-parameter simultaneous measurement, three independent resonant peaks were selected in this paper. Based on the theoretical analysis and experimental observations, the chosen peaks are the Bragg wavelength peak and the 25th- and 28th-order cladding resonance peaks. These cladding modes belong to high-order modes and are close to the cut-off wavelength, which make them sensitive to the refractive index within a measurement range of 1.344 to 1.427. Taking these factors into account, the sensitivity matrix for measuring the temperature, axial strain, and SRI by means of TFBG can be expressed as

$$\begin{pmatrix}\Delta\lambda_B\\ \Delta\lambda_{cl}^{25}\\ \Delta\lambda_{cl}^{28}\end{pmatrix}=\begin{pmatrix}K_{B,T},K_{B,\varepsilon},0\\ K_{cl,T}^{25},K_{cl,\varepsilon}^{25},K_{cl,n_{\text{ext}}}^{25}\\ K_{cl,T}^{28},K_{cl,\varepsilon}^{28},K_{cl,n_{\text{ext}}}^{28}\end{pmatrix}\begin{pmatrix}\Delta T\\ \Delta\varepsilon\\ \Delta n_{\text{ext}}\end{pmatrix}, \tag{5}$$

where $\Delta\lambda_B$, $\Delta\lambda_{cl}^{25}$, and $\Delta\lambda_{cl}^{28}$ are the wavelength shifts of the core mode resonance and the cladding mode resonances, respectively. Each coefficient in the matrix can be obtained through experimental observations. Thus, the temperature, axial strain, and SRI can be calculated by reversely solving the above-mentioned equation, expressed as

$$\begin{pmatrix}\Delta T\\ \Delta\varepsilon\\ \Delta n_{\text{ext}}\end{pmatrix}=\begin{pmatrix}K_{B,T},K_{B,\varepsilon},0\\ K_{cl,T}^{25},K_{cl,\varepsilon}^{25},K_{cl,n_{\text{ext}}}^{25}\\ K_{cl,T}^{28},K_{cl,\varepsilon}^{28},K_{cl,n_{\text{ext}}}^{28}\end{pmatrix}^{-1}\begin{pmatrix}\Delta\lambda_B\\ \Delta\lambda_{cl}^{25}\\ \Delta\lambda_{cl}^{28}\end{pmatrix}. \tag{6}$$

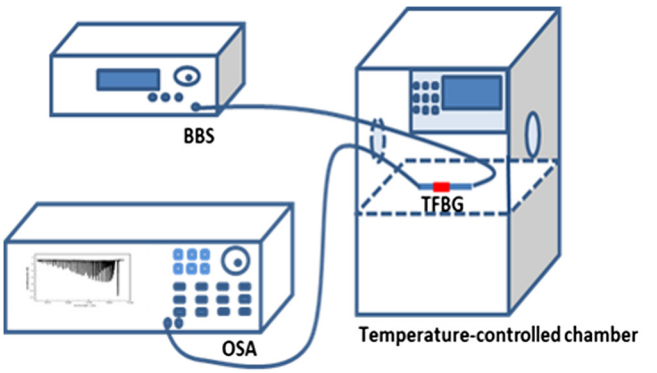

Fig. 3 Schematic diagram of experimental setup for temperature measurement using TFBG.

3 Experiment and Result

A photosensitive single-mode fiber (SMF; core diameter of 8.2 μm, cladding diameter of 125 ± 0.7 μm, and numerical aperture of 0.14) hydrogen-loaded under a pressure of 13 Kpa for 14 days was used to fabricate the TFBG using the phase mask method. The TFBG was written by scanning an ultraviolet light from a 248-nm KrF excimer laser on the photosensitive SMF via a uniform phase mask for a period of 1347.30 nm. Different from the ordinary FBG writing method, the phase mask must be tilted at a certain angle while writing TFBG so the grating plane can be tilted to a certain degree with respect to the optical fiber transmission axis. The effective tilt angle in this experiment was 2 deg, and the TFBG was 2-cm long.

First, temperature measurement based on the TFBG was performed. An optical broadband source was used to emit light into the fabricated TFBG, and the transmission spectrum was detected using an optical spectrum analyzer (OSA, YOKOGAWA AQ6375) at a resolution of 0.046 nm. The TFBG was placed in the temperature-controlled chamber as shown in Fig. 3.

The measuring range in the experiment was 28°C to 80°C, and the resolution of the temperature increment was 0.1°C. The wavelength shifts of the core mode and cladding mode resonant peaks at different temperatures were determined by a spectrometer as shown in Fig. 4. As described in Sec. 2, the resonant peaks of the core mode and cladding modes

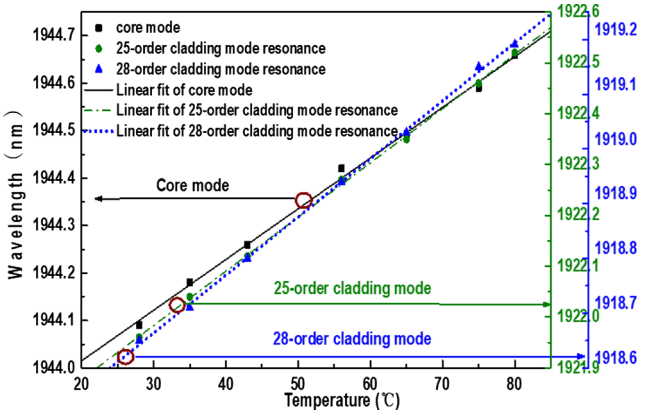

Fig. 4 Evolutions of resonant wavelengths of the core mode and 25th- and 28th-order cladding modes of TFBG with temperature increases and linear fitting of the corresponding data.

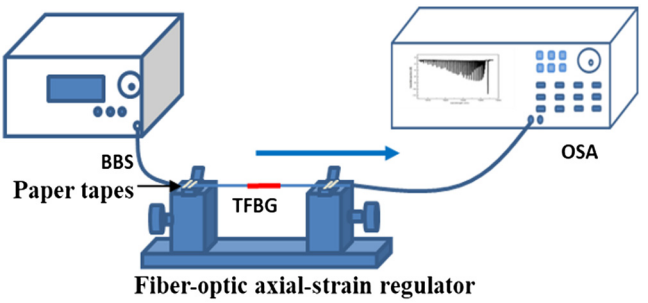

Fig. 5 Schematic diagram of experimental configuration of TFBG axial-strain measurement.

moved toward a longer wavelength as the temperature increased. Due to the low thermal expansion coefficient and thermo-optic coefficient, the wavelength shift difference induced by the change in temperature between the resonant peaks of the core mode and cladding modes was small. As shown in Fig. 3, the slope of the fitted curves was 0.01069, 0.01065, and 0.0106, respectively; the goodness of linear fitting was 0.997, 0.999, and 0.999, respectively.

Second, the axial-strain measurement based on the TFBG was performed. The schematic diagram of the experimental setup used for axial-strain measurement is shown in Fig. 5.

Because the clamps of the fiber-optic axial-strain regulator were tight and could potentially damage the fiber, this experiment used paper tapes to affix the TFBG to the regulator to avoid introducing additional loss. Each side of the TFBG was fastened using two pieces of paper tape to ensure that the fiber was firmly placed. Then, the TFBG could be stretched in one direction by adjusting the axial-strain regulator. The resonant peaks of the core mode and cladding modes drifting with strain are shown in Fig. 6. As strain increased, the resonant peaks of the core mode and the 25th- and 28th-order cladding modes moved toward a longer wavelength to slightly different degrees. As shown in Fig. 6, the slopes for the fitting lines demonstrated extremely small differences: 0.000992, 0.000947, and 0.000942, respectively. Given that the chosen cladding modes were close to each other, the difference of the photoelastic coefficients was quite small, leading to slightly different dependences of each

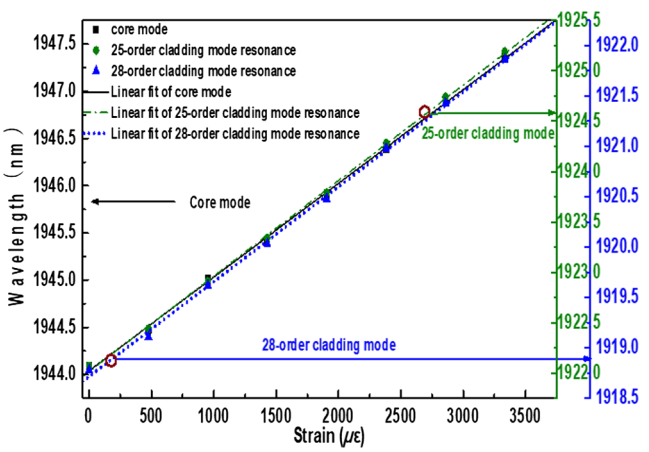

Fig. 6 Spectral responses of resonant wavelengths of the core mode and 25th- and 28th-order cladding modes of TFBG with axial strain increases and the linear fitting of corresponding data.

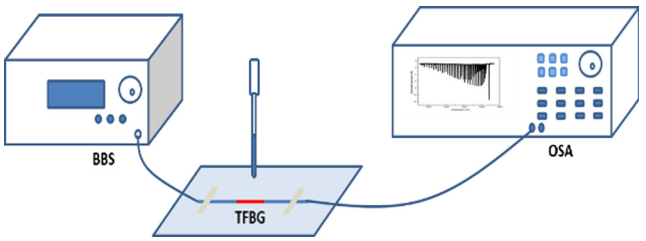

Fig. 7 Experimental structure schematic diagram of refractive measurement using TFBG.

mode on the same axial strain. The goodness of linear fitting was 0.999, 0.999, and 0.999, respectively.

Then, SRI measurement based on the TFBG was conducted. The grating was placed horizontally on a flat plate and titrated using glycerol solutions at different concentrations as shown in Fig. 7.

After taking every measurement of the glycerol solution concentration, the TFBG was titrated to wash with pure water before being sufficiently dried to guarantee no residual glycerin solution on the surface of the TFBG and to ensure the transmission spectrum returned to the original state.

The transmission spectrum of the TFBG for different SRIs is shown in Fig. 8. The cladding resonant peaks presented continuous wavelength drift with an increase in the solution concentration. Within a large range of SRI change, the overall trend of wavelength drift varied exponentially but varied nearly linearly within a certain SRI range from 1.398 to 1.420 as shown in Figs. 9 and 10, respectively. The other cladding modes exhibited the same properties, and other resonances could thus also be chosen as the investigated peaks. As shown in Fig. 9, the slopes of the fitting lines for the 25th- and 28th-order cladding mode resonance in a specific SRI range (i.e., 1.398 to 1.420) were 8.0931 and 10.8689, respectively, and the goodness of linear fitting was 0.998 and 0.992. Figure 9 shows that the Bragg wavelength remained nearly unchanged and was insensitive to SRI variation, consistent with theoretical analysis.

The above analysis shows that all parameters in the sensitivity coefficient matrix were determined experimentally. Using Eq. (6), the change in temperature, strain, and SRI can be calculated from the following matrix:

$$\begin{pmatrix} \Delta T \\ \Delta \varepsilon \\ \Delta n_{\text{ext}} \end{pmatrix} = \begin{pmatrix} 0.01069, 0.000992, 0 \\ 0.01065, 0.000947, 8.093 \\ 0.0106, 0.000942, 10.869 \end{pmatrix}^{-1} \begin{pmatrix} \Delta\lambda_B \\ \Delta\lambda_{cl}^{25} \\ \Delta\lambda_{cl}^{28} \end{pmatrix}. \tag{7}$$

4 Discussion

Table 1 lists the comparison of temperature, strain, and SRI sensitivities in this paper with results at 1550 nm reported in other papers. For certain sensitivity parameters, such as temperature sensitivity in Ref. 15, the sensors working in the 1550-nm band demonstrated superiority over that shown in this paper, presumably due to the larger transmission loss around the 2-μm band. However, the overall sensing performance of the proposed structure appears acceptable for explorative work in a new band. In addition to exhibiting comparable sensing performance, the TFBG sensor in the 2-μm band demonstrated other advantages. First, in most

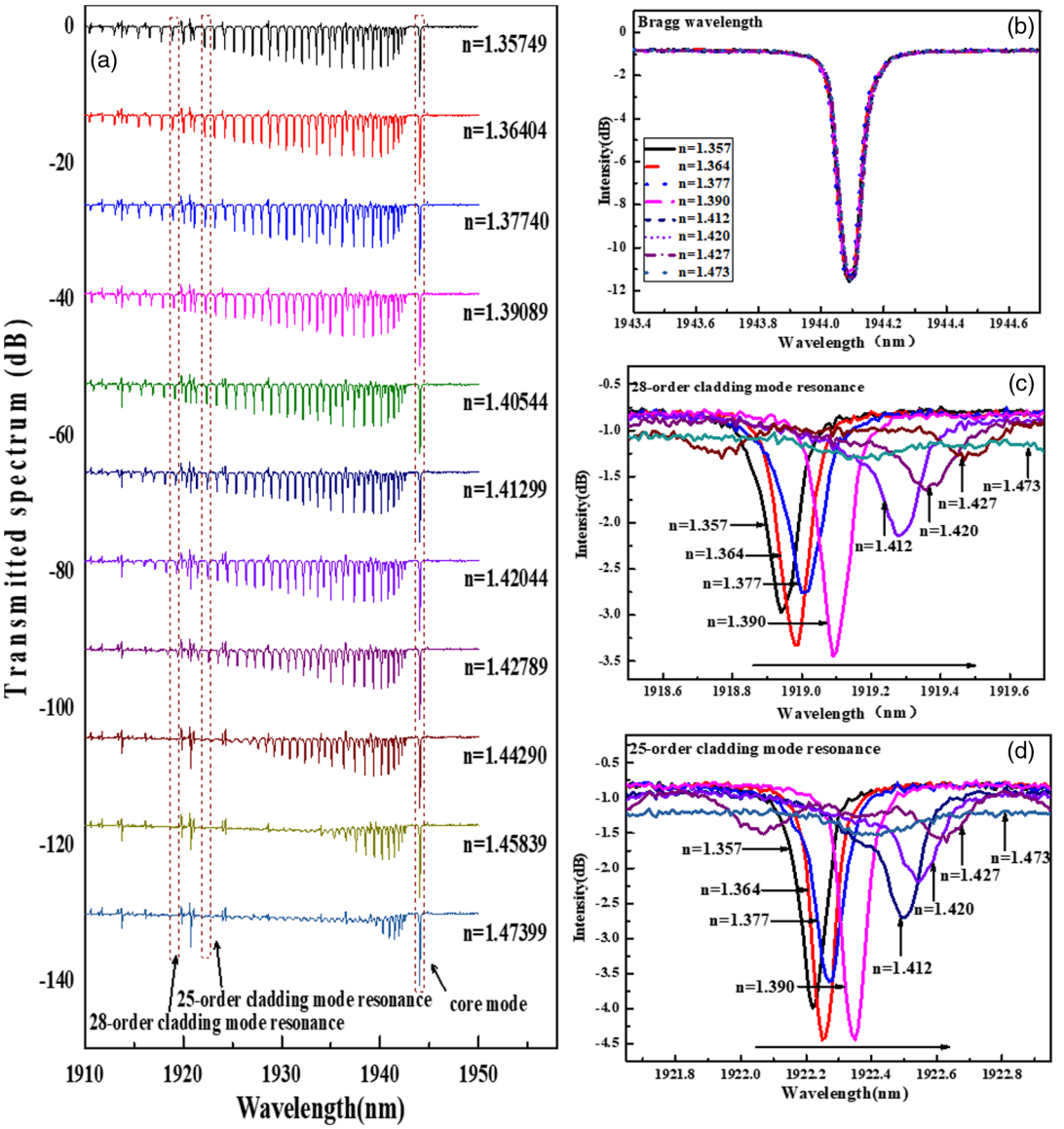

Fig. 8 (a) Whole-transmission spectral response evolution of TFBG titrated by glycerol solutions with SRIs from 1.357 to 1.474, (b) change of core mode with SRI from 1.357 to 1.474, (c) change of 25th-order cladding modes with SRIs from 1.357 to 1.474, and (d) change of 28th-order cladding modes with SRIs from 1.357 to 1.474.

studies on TFBG, SRI was measured using an area-detection or power-detection method. This paper employs the wavelength demodulation method, which is simpler and more convenient. Second, the measuring efficiency was improved using the proposed algorithm. Three-parameter simultaneous measurement in the 1550-nm band[30] was realized by measuring SRI sensitivity first and then using a 2×2 matrix to further calculate the strain and temperature sensitivity. Different from the two-step algorithm, the proposed algorithm can achieve simultaneous measurement with only a 3×3 matrix. Finally, this method also reduces the complexity of experimental facilities, which is economical and can minimize loss and error in the experimental process.

5 Conclusion

In this paper, an optical fiber sensor operating in a 2-μm band based on a single TFBG to achieve simultaneous measurements of temperature, axial strain, and SRI is analyzed theoretically and demonstrated experimentally for the first time. The wavelength drift of the cladding modes showed a good linear relationship with changes in temperature, strain, and SRI in a certain range, whereas the Bragg wavelength shifted linearly with changes in temperature and strain but were insensitive to SRI. By measuring the drift of three independent resonance wavelengths, the variations of temperature ΔT, stress $\Delta\varepsilon$, and SRI Δn_{ext} could be determined using a 3×3 sensitivity matrix. The sensor operating in the 2-μm band was found to possess advantages of simple structure, low cost, and easy operation. In subsequent research, the authors will continue to increase the tilt angle of the present TFBG or use other photosensitive fiber-written TFBGs to expand the SRI measurement range.

Acknowledgments

This work was supported by the Fundamental Research Funds for the Central Universities (No. 2017YJS012).

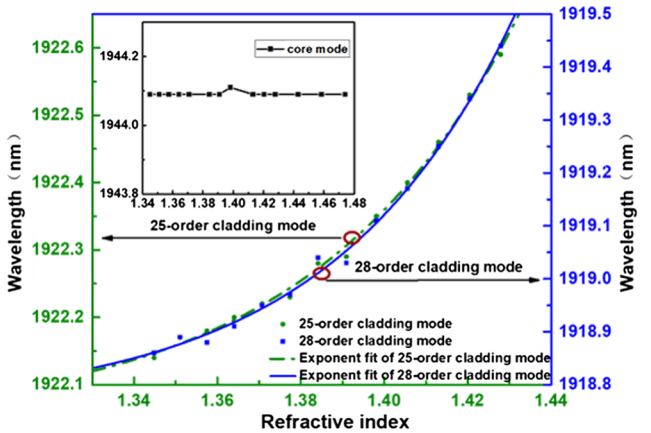

Fig. 9 Measured results of resonant wavelengths for the 25th- and 28th-order cladding modes of TFBG versus SRIs within the whole measuring range from 1.344 to 1.473 and the fitting curves of corresponding data. Inset shows the core mode resonant wavelength shift response in the whole SRI range.

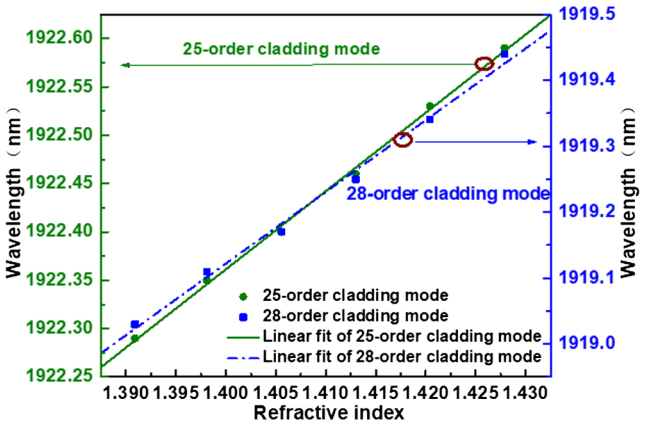

Fig. 10 Measured results of resonant wavelengths for the 25th- and 28th-order cladding modes of TFBG versus SRIs within a range from 1.390 to 1.427 and the linear fitting curve for corresponding data.

Table 1 Comparison of temperature, axial strain, and SRI sensitivity with sensing results at 1550 nm.

	Temperature (pm/°C)		Axial strain (pm/$\mu\varepsilon$)		SRI (nm/RIU)
Resonance mode	λ_B	λ_{cl}^i	λ_B	λ_{cl}^i	λ_{cl}^i
This paper	10.69	10.65	0.996	0.942	10.869
Reference 29	10	10	0.636	0.667	
Reference 30	8.5	9.8	1.03	1.03	
Reference 15	11.42	11.4			10.843

References

1. G. Jihong et al., "Development of eye-safe fiber lasers near 2 μm," *IEEE J. Sel. Top. Quantum Electron.* **20**(5), 150–160 (2014).
2. A. Ghosh et al., "All-fiber tunable ring laser source near 2 μm designed for CO_2 sensing," *Sens. Actuators B: Chem.* **235**, 547–553 (2016).
3. N. M. Fried and K. E. Murray, "High-power thulium fiber laser ablation of urinary tissues at 1.94 μm," *J. Endourol.* **19**(1), 25–31 (2005).
4. S. W. Henderson et al., "Eye-safe coherent laser radar system at 2.1 μm using Tm, Ho:YAG lasers," *Opt. Lett.* **16**(10), 773–775 (1991).
5. T. M. Taczak and D. K. Killinger, "Development of a tunable, narrow-linewidth, cw 2.066-μm Ho:YLF laser for remote sensing of atmospheric CO_2 and H_2O," *Appl. Opt.* **37**(36), 8460–8476 (1998).
6. Y. Ren et al., "2 μm mode-locking laser performances of sol-gel-fabricated large-core Tm-doped silica fiber," *Chin. Opt. Lett.* **16**(2), 020020 (2018).
7. J. Qiao et al., "High-quality 2-μm Q-switched pulsed solid-state lasers using spin-coating-coreduction approach synthesized Bi_2Te_3 topological insulators," *Photonics Res.* **6**(4), 314–320 (2018).
8. S. S. Lindsay et al., "The red edge problem in asteroid band parameter analysis," *Meteorit. Planet. Sci.* **51**(4), 806–817 (2016).
9. B. Jiang et al., "Carbon nanotube-deposited tilted fiber Bragg grating for refractive index and temperature sensing," *IEEE Photonics Technol. Lett.* **28**(9), 994–997 (2016).
10. J. Albert, "Tilted fiber Bragg gratings as multi-sensors," *Opt. Photonics News* **22**(10), 28–33 (2011).
11. C. H. Yeh et al., "Utilizing simple FBG-based erbium-doped fiber architecture for remote temperature sensing," *Laser Phys.* **25**(10), 105102 (2015).
12. G. Woyessa et al., "Zeonex-PMMA microstructured polymer optical FBGs for simultaneous humidity and temperature sensing," *Opt. Lett.* **42**(6), 1161–1164 (2017).
13. R. Xu, A. Yurkewich, and R. V. Patel, "Curvature, torsion, and force sensing in continuum robots using helically wrapped FBG sensors," *IEEE Rob. Autom. Lett.* **1**(2), 1052–1059 (2016).
14. B. Yang et al., "Fibre optic sensing based slope crest tension crack monitoring system for surface mines," in *2nd Int. Conf. for Fibre-optic and Photonic Sensors for Industrial and Safety Applications (OFSIS)*, pp. 27–32 (2017).
15. Y. Miao et al., "Simultaneous measurement of surrounding temperature and refractive index by the tilted fiber Bragg grating," *Proc. SPIE* **7134**, 71343W (2008).
16. D. Wada, H. Igawa, and H. Murayama, "Simultaneous distributed measurement of the strain and temperature for a four-point bending test using polarization-maintaining fiber Bragg grating interrogated by optical frequency domain reflectometry," *Measurement* **94**(Suppl. C), 745–752 (2016).
17. T. Osuch et al., "Simultaneous measurement of liquid level and temperature using tilted fiber Bragg grating," *IEEE Sens. J.* **16**(5), 1205–1209 (2016).
18. L. Qi et al., "Highly reflective long period fiber grating sensor and its application in refractive index sensing," *Sens. Actuators B: Chem.* **193**, 185–189 (2014).
19. Y. Miao et al., "Temperature-insensitive refractive index sensor based on tilted fiber Bragg grating," *Microwave Opt. Technol. Lett.* **51**(2), 479–483 (2009).
20. Q. Jiang, "A novel oil level monitoring sensor based on string tilted fiber Bragg grating," *Optoelectron. Lett.* **7**(3), 171–174 (2011).
21. M. Li et al., "Continuously tunable photonic fractional temporal differentiator based on a tilted fiber Bragg grating," *IEEE Photonics Technol. Lett.* **23**(4), 251–253 (2011).
22. Q. Jiang, "A comparison study of the sensing characteristics of FBG and TFBG," *Sens. Rev.* **33**(1), 68–79 (2013).
23. C. Shen et al., "Tilted fiber Bragg gratings and its fiber humidity and twist sensing applications," in *15th Int. Conf. on Optical Communications and Networks (ICOCN)*, pp. 1–3 (2016).
24. X. Chen et al., "Wide range refractive index measurement using a multi-angle tilted fiber Bragg grating," *IEEE Photonics Technol. Lett.* **29**(9), 719–722 (2017).
25. C. Caucheteur et al., "External refractive index sensitivity of weakly tilted fiber Bragg gratings with different coating thicknesses," *IEEE Sens. J.* **8**(7), 1330–1336 (2008).
26. J. Yang et al., "Relative humidity sensor based on optical fiber gratings and polyvinyl alcohol," in *7th IEEE/Int. Conf. on Advanced Infocomm Technology*, pp. 137–142 (2014).
27. Y. C. Lu, W. P. Huang, and S. S. Jian, "Polarization sensitivities of demodulation techniques for tilted fiber Bragg Grating refractometer," in *Asia Communications and Photonics Conf. and Exhibition (ACP)*, pp. 1–7 (2009).
28. B. Gu et al., "Simple and compact reflective refractometer based on tilted fiber Bragg grating inscribed in thin-core fiber," *Opt. Lett.* **39**(1), 22–25 (2014).
29. W.-H. Zhang et al., "Temperature and strain sensing characteristics of the tilted fiber Bragg grating," *Optoelectron. Lett.* **6**(5), 355–358 (2010).
30. N. J. Alberto et al., "Three parameters simultaneous measurement with a single TFBG," in *21st Int. Conf. on Optical Fiber Sensors* (2011).

Dan Cheng received her BE degree in communication and information systems from Tianjin Polytechnic University, China, in 2015. Since then, she has been a PhD candidate at the Institute of Lightwave Technology, Beijing Jiaotong University, China. Her current research interests include thulium-doped fiber lasers, fiber optics, and optical communications. He is with the Key Laboratory of All Optical Network and Advanced Telecommunication of Electromagnetic

Compatibility, Institute of Lightwave Technology, Beijing Jiaotong University, Beijing, China.

Fengping Yan is with the Key Laboratory of All Optical Network and Advanced Telecommunication of Electromagnetic Compatibility, Institute of Lightwave Technology, Beijing Jiaotong University, Beijing, China.

Feng Ting is with the Hebei Key Laboratory of Optic-Electronic Information and Materials, Photonics Information Innovation Center, College of Physics Science and Technology, Baoding, China.

Zhuoya Bai is with the Key Laboratory of All Optical Network and Advanced Telecommunication of Electromagnetic Compatibility, Institute of Lightwave Technology, Beijing Jiaotong University, Beijing, China.

Luna Zhang is with the Key Laboratory of All Optical Network and Advanced Telecommunication of Electromagnetic Compatibility, Institute of Lightwave Technology, Beijing Jiaotong University, Beijing, China.

Wei Wang is with the Key Laboratory of All Optical Network and Advanced Telecommunication of Electromagnetic Compatibility, Institute of Lightwave Technology, Beijing Jiaotong University, Beijing, China.

Shuo Liu is with the School of Electronic Information Engineering, Hebei University of Technology, Tianjin, China.

Hong Zhou is with the Department of Electronics, Information and Communication Engineering, Osaka Institute of Technology, Osaka, Japan.

Yafei Hou is with the Graduate School of Natural Science and Technology, Okayama University, Okayama, Japan.